6th ECCOMAS Conference on Smart Structures and Materials
SMART2013
Politecnico di Torino, 24-26 June 2013
E. Carrera, F. Miglioretti and M. Petrolo (Editors)
www.smart2013.com

DETECTION AND LOCALISATION OF DAMAGE ON INDUSTRIALLY PRODUCED CONCRETE SLABS THROUGH TIME- AND FREQUENCY-DOMAIN APPROACHES

Viet Ha Nguyen [*], Jean Mahowald [*], Jean-Claude Golinval [†], Stefan Maas [*]

[*] University of Luxembourg
Faculty of Science, Technology and Communication
Rue Coudenhove – Kalergi 6, L – 1359 Luxembourg
e-mail of the corresponding author: vietha.nguyen@uni.lu

[†] University of Liege (ULg)
Department of Aerospace and Mechanical Engineering
LTAS-Vibrations et Identification des Structures
Chemin des Chevreuils 1, B 52, B - 4000 Liège 1, Belgium

Key words: identification, damage detection, localization

Summary: *The objective of this work is to address the problem of damage detection in civil engineering structures using non-destructive techniques and dynamic measurements. To this purpose, time- or frequency-domain methods are used for the diagnostics. It consists in practical output-only techniques as Stochastic Subspace Identification (SSI) for modal identification or Enhanced Principal Component Analysis (EPCA) for detecting the presence of damage. The use of the Hankel matrix instead of the observation matrix improves effectively the robustness of these methods. Damage localization is based on Frequency Response Functions (FRFs) and sensitivity analysis of PCA results.*

The efficiency of the above-mentioned methods has been demonstrated in earlier studies mainly on numerical models and small-scale laboratory experiments [3, 4]. It was also tested successfully on industrial examples to perform machine condition monitoring using a reduced set of sensors [2]. In this work, the investigation is performed on precast prestressed and non-prestressed concrete slabs. Successive damages were artificially introduced in the slabs by loading heavy weights and by cutting steel wires, which induced cracks in the structure. The examples show the consequences of the considered techniques for damage identification. The results that are very different between prestressed and non-prestressed slabs may be used as input for the condition control of this kind of structures.

1 INTRODUCTION

For a few years, the detection, localization and assessment of damage in mechanical structures have attracted the attention of numerous engineering researchers. Remote

approaches not only allow guaranteeing safety but also reducing effectively maintenance and repair costs. Generally, detection is based on monitoring structural features such as modal parameters.

In the time-domain, several methods are popular because they are straightforward in extracting structural characteristics from output-only measurements. They have been proven efficient for the purpose of modal analysis, e.g. Stochastic Subspace Identification (SSI), Principal Component Analysis (PCA) or Second-Order Blind Identification (SOBI) etc. [1, 2]. For the purpose of damage detection or fault diagnosis, improved PCA versions exist based on the use of Hankel matrices instead of the observation matrix e.g. Enhanced PCA and Null Subspace Analysis (NSA) [3, 4].

Modal identification in the frequency-domain is also popular e.g. the Frequency Domain Decomposition (FDD) and Least Squares Complex Frequency-Domain (LSCF) estimation methods. More recently, the PolyMax has been proposed [5] and shows very attractive for civil and industrial applications [6-8].

The objective of the present paper is to perform a comparison between several current detection methods. For modal identification and detection, the SSI, Enhanced PCA and PolyMax methods are considered. A sensitivity analysis for PCA in the frequency domain and an experimental estimation of the flexibility matrix are adopted for damage localization. The methods are applied on data obtained from precast concrete slabs, one purely reinforced and one prestressed slab.

2 STRUCTURAL FEATURE EXTRACTION BY SUBSPACE IDENTIFICATION

Let $\mathbf{H}$ be the Hankel matrix constructed from vibration measurements $\left[\mathbf{x}_1\ \mathbf{x}_2 \ldots \mathbf{x}_k \ldots \mathbf{x}_N\right]$ where $\mathbf{x}_k \in \mathbb{R}^m$ is the output vector at time step k, m is the number of output sensors and N is the number of time samples.

$$\mathbf{H}_{1,2i} = \left[\begin{array}{ccccc} \mathbf{x}_1 & \mathbf{x}_2 & \ldots & \ldots & \mathbf{x}_j \\ \mathbf{x}_2 & \mathbf{x}_3 & \ldots & \ldots & \mathbf{x}_{j+1} \\ \ldots & \ldots & \ldots & \ldots & \ldots \\ \mathbf{x}_i & \mathbf{x}_{i+1} & \ldots & \ldots & \mathbf{x}_{i+j-1} \\ \hline \mathbf{x}_{i+1} & \mathbf{x}_{i+2} & \ldots & \ldots & \mathbf{x}_{i+j} \\ \mathbf{x}_{i+2} & \mathbf{x}_{i+3} & \ldots & \ldots & \mathbf{x}_{i+j+1} \\ \ldots & \ldots & \ldots & \ldots & \ldots \\ \mathbf{x}_{2i} & \mathbf{x}_{2i+1} & \ldots & \ldots & \mathbf{x}_{2i+j-1} \end{array}\right] \equiv \left[\begin{array}{c} \mathbf{H}_p \\ \hline \mathbf{H}_f \end{array}\right] \equiv \begin{array}{c} "past" \\ \hline "future" \end{array} \qquad (1)$$

where $2i$ is a user-defined number of row blocks, whereas each block contains m rows (number of measurement sensors), j is the number of columns (practically $j = N\text{-}2i\text{+}1$). The

Hankel matrix $\mathbf{H}_{1,2i}$ consists of $2im$ rows and is split into two equal parts of i block rows, which represent past and future data respectively and enable to take into account time correlation between measurements. A singular value decomposition (SVD) on the Hankel matrix leads to:

$$\mathbf{H}_{1,2i} = \mathbf{U}\boldsymbol{\Sigma}\mathbf{V}^{\mathrm{T}} \approx \begin{bmatrix}\mathbf{U}_1 & \mathbf{U}_2\end{bmatrix}\begin{bmatrix}\boldsymbol{\Sigma}_1 & \mathbf{0} \\ \mathbf{0} & \mathbf{0}\end{bmatrix}\begin{bmatrix}\mathbf{V}_1 & \mathbf{V}_2\end{bmatrix}^{\mathrm{T}} = \mathbf{U}_1\boldsymbol{\Sigma}_1\mathbf{V}_1^{\mathrm{T}} \tag{2}$$

where diagonal matrix $\boldsymbol{\Sigma}_1$ involves $p \approx 2n_m$ non-zero singular values in decreasing order and n_m is the number of vibrating modes.

From active components $\mathbf{U}_1$, $\boldsymbol{\Sigma}_1$ and $\mathbf{V}_1$, the Stochastic Subspace Identification (SSI) allows extracting modal parameters such as natural frequencies, damping ratios and mode shapes. It is worth noting that the model order p is not always explicitly determined because apart from $\boldsymbol{\Sigma}_1$, remaining diagonal elements of $\boldsymbol{\Sigma}$ are not completely null due to noise or set-up and computational errors. Therefore, the construction of a stabilization diagram is useful based on identified frequencies and damping ratios corresponding to a series of increasing model orders p. This facilitates the distinction between physical and spurious numerical modes. More detailed information on SSI operation can be found in [1].

The structural health of the structure can be monitored by comparing identified modal parameters from the reference (healthy) and the current states respectively. Alternatively, damage detection may be performed without performing the modal identification step, as in the Enhanced Principal Component Analysis (EPCA) method [4]. In this case, the dynamic state of the structure may be characterized by principal components – the column vectors of matrix $\mathbf{U}_1$ defining the 'active subspace' for the state. Hence, the comparison between two different states may be implemented directly using the subspaces spanned by principal components according to each state. A useful tool to perform such comparison is the *concept of subspace angle* [9]. In the absence of damage or variation of environmental conditions, the characteristic subspace $\mathbf{U}_1$ remains unchanged. Any change in the dynamic behaviour caused by a modification of the system state modifies consequently its characteristic subspace.

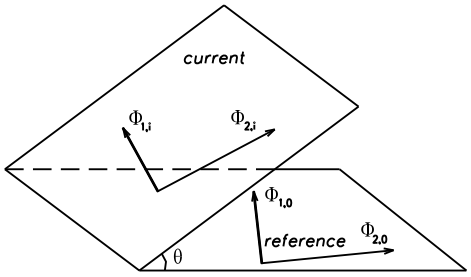

Figure 1 - Angle θ formed by active subspaces according to the reference and current states, due to a dynamic change

As illustrated by a two-dimensional case in Figure 1, the concept of subspace angle can be seen as a tool to quantify existing spatial coherence between two data sets resulting from

observations of a vibrating system. In Figure 1, an active subspace is built from two principal components.

3 MODAL ANALYSIS IN THE FREQUENCY DOMAIN USING POLYMAX

The PolyMax method makes use of measured Frequency Response Functions (FRFs) as input data. For a system with *r* inputs and *m* outputs, the FRF matrix can be expressed by the modal decomposition:

$$\mathbf{H}(\omega) = \sum_{k=1}^{n_m} \frac{\phi_k \gamma_k^{\mathrm{T}}}{j\omega - \lambda_k} + \frac{\bar{\phi}_k \gamma_k^{\mathrm{H}}}{j\omega - \bar{\lambda}_k} + \mathrm{UR} - \frac{\mathrm{LR}}{\omega^2} \tag{3}$$

where n_m is number of modes; $\phi_k \in \mathbb{C}^m$ are the mode shapes; $\gamma_k^{\mathrm{T}} \in \mathbb{C}^r$ are the modal participation factors and λ_k are the poles which relate to the eigenfrequencies ω_k and damping ratios ζ_k by $\lambda_k, \bar{\lambda}_k = -\zeta_k \omega_k \pm j\sqrt{1-\zeta_k^2}\,\omega_k$. A bar denotes the complex conjugate and $\bullet^{\mathrm{H}}$ is the complex conjugate transpose of a matrix. The upper and lower residuals UR, LR $\in \mathbb{R}^{m \times r}$ are introduced to model the influence of the out-of-band modes in the considered frequency band. Detailed information on the PolyMax method can be found in [6].

As for the SSI method, true physical modes may be picked from a stabilization diagram. In comparison with SSI, the PolyMax stabilization diagram is much clearer as explained in [6].

4 DAMAGE LOCALIZATION

4.1 Method based on flexibility

A popular method to locate damage from modal features is based on flexibility (or/and stiffness) analysis from measured mode shapes [10, 11]. The experimental flexibility matrix, which is the inverse of the stiffness matrix, can be evaluated in terms of mass-normalized mode shapes ϕ_k ($\Phi^{\mathrm{T}}\mathbf{M}\Phi = \mathbf{I}$ that $\mathbf{M}$ is the mass matrix) corresponding to angular eigenfrequencies ω_k :

$$\mathbf{F} = \sum_{k=1}^{n_m} \frac{1}{\omega_k^2} \phi_k . \phi_k^{\mathrm{T}} \tag{4}$$

Change in the measured flexibility matrix of a current state with respect to the reference state may reveal the position of damage. The comparison can be performed from the diagonal elements of the flexibility matrices in varied conditions. Alternatively, another damage indicator consists in observing the maximum value of each column of flexibility difference [12]:

$$\Delta\mathbf{F} = \left\{\delta_{ij}\right\} = \mathbf{F}^d - \mathbf{F}^r \qquad \delta_i = \max\left|\delta_{ij}\right| \tag{5}$$

where $\mathbf{F}^d$ and $\mathbf{F}^r$ denote the flexibility matrices in a current state and the reference state respectively.

A relative difference can be also evaluated for maximizing useful information as follows:

$$\text{rel}F_{ij} = \frac{F_{ij}^d - F_{ij}^r}{F_{ij}^r} \cdot 100\% \tag{6}$$

This relative difference allows improving the visualization of change, however, large numerical errors may occur at some specific positions when the denominator values F_{ij}^r are small (e.g. around bearings). In this case, a threshold on the denominator may be introduced for nodes around bearings. In this work, only values of F_{ij}^d for which F_{ij}^r is in the range of 10 to 100% of the maximal value of $\mathbf{F}^r$ are taken into account. Other values are set to 0, leading to the disadvantage that damage close to supports or bearings is not detectable with this relative indicator.

4.2 Method based on sensitivity analysis

Damage localization can also be carried out by sensitivity analysis of PCA modes in the frequency-domain [13].

Let us consider the FRFs $\mathbf{H}^s(\omega)$ for a single input at location *s*:

$$\mathbf{H}^s(\omega) = \begin{bmatrix} h(\omega_1) & h(\omega_2) & \dots & h(\omega_N) \end{bmatrix} \tag{7}$$

where vector $h(\omega_k)$ is of dimension *m* (the number of measured co-ordinates) and *N* is the number of frequency lines. The rows of $\mathbf{H}^s$ represent the responses at the measured degrees of freedom (DOFs), while the columns are "snapshots" of the FRFs at different frequencies. We will assume that the dynamical system matrices depend on a vector of parameters *p*. This vector of parameters may consist of system parameters or state variables. We can assess its principal components through Singular Value Decomposition (SVD):

$$\mathbf{H}^s = \mathbf{U}\boldsymbol{\Sigma}\mathbf{V}^{\mathrm{T}} \tag{8}$$

As $\mathbf{H}^s$ belongs to the frequency-domain, the left singular vectors in $\mathbf{U}$ give spatial information, the right singular vectors in $\mathbf{V}$ represent modulation functions depending on frequency and the diagonal matrix of singular values $\boldsymbol{\Sigma}$ contains scaling parameters of descending order $\sigma_1 > \sigma_2 > \ldots > \sigma_m$. In other words, the SVD of $\mathbf{H}^s$ separates information depending on space and frequency.

From Equation (8), a sensitivity analysis can be performed by taking the derivative of the observation matrix with respect to *p*:

$$\frac{\partial \mathbf{H}^s}{\partial p} = \frac{\partial \mathbf{U}}{\partial p}\boldsymbol{\Sigma}\mathbf{V}^{\mathrm{T}} + \mathbf{U}\frac{\partial \boldsymbol{\Sigma}}{\partial p}\mathbf{V}^{\mathrm{T}} + \mathbf{U}\boldsymbol{\Sigma}\frac{\partial \mathbf{V}^{\mathrm{T}}}{\partial p} \tag{9}$$

Through this equation, the sensitivity of the system dynamic response shows its dependence on the sensitivity of each SVD term. Junkins and Kim [14] developed a method to compute the partial derivatives of SVD factors. Here for the sake of localization, we are more particularly interested in spatial information contained in the left singular vector **U**; its sensitivity with respect to a given parameter p_k is simply given by the following equation:

$$\frac{\partial U_i}{\partial p_k} = \sum_{j=1}^{m} \alpha_{ji}^k U_j \quad \text{with} \quad \alpha_{ji}^k = \frac{1}{\sigma_i^2 - \sigma_j^2} \left[\sigma_i \left(U_j^{\mathrm{T}} \frac{\partial \mathbf{H}^s}{\partial p_k} V_i \right) + \sigma_j \left(U_i^{\mathrm{T}} \frac{\partial \mathbf{H}^s}{\partial p_k} V_j \right)^{\mathrm{T}} \right] \tag{10}$$

It is shown in [14] that the diagonal coefficients α_{ii}^k keep only their imaginary part (their real parts are empty). So, the sensitivity of the *i*th principal component can be computed through coefficients α_{ji}^k which depend on an unknown $\partial \mathbf{H}^s / \partial p_k$. It is proven in [4] that when the system matrices are symmetric, if the parameter of interest is some coefficient k_e of the stiffness matrix, the sensitivity of the FRF matrix may be simply determined by the following equation

$$\partial \mathbf{H}^s / \partial p_k = -H_{k_e} . H_{k_e,s} \tag{11}$$

where H_{k_e} is just the row vector corresponding to coefficient k_e of the FRF matrix in equation (7) and $H_{k_e,s}$ is the *s* element of this vector.

Once $\partial \mathbf{H}^s / \partial p_k$ has been computed, the sensitivity of the left singular vectors is a good candidate for resolving localization problems of linear-form structures, e.g. chain-like or beam-like structures. In each working condition of the system, we can compute the sensitivity $\partial U_i / \partial p_k$. The reference state is denoted by $\partial U_i^R / \partial p_k$, and the deviation of the current condition may be assessed as follows:

$$\Delta \frac{\partial U_i}{\partial p_k} = \frac{\partial U_i}{\partial p_k} - \frac{\partial U_i^R}{\partial p_k} \tag{12}$$

The last vector allows the maximization of useful information for damage localization.

5 DAMAGE DETECTION ON PRECAST CONCRETE SLABS

5.1 Description of the panels

The two investigated panels are manufactured by the company ECHOLUX and both are of the same type (VSF-15-120, one prestressed concrete (PC) slab, one specially fabricated non-prestressed passively reinforced concrete (RC) slab for testing purposes only). Hence, there were two apparently identical slabs but one simply not prestressed. They are made of concrete C50/60 with an elastic modulus of 42700 N/mm^2 and a measured compressive strength of 58.3N/mm^2 (quality control of manufacturer). The quality of the reinforcement is St 1470/1670 and the corresponding elastic modulus 205000N/mm^2. In the upper section of the panel, there are 4 wires with a diameter of 5mm and in the lower section 12 wires with a

diameter of 7mm. Before testing, the concrete at the bottom side in the middle of the slab along axis C (Figure 2b) was removed, as shown in Figure 2a, to give access to the reinforcement for the later procedures of cutting tendons.

Both static and dynamic tests were performed on the slabs to compare their behavior in each condition [15]. The dynamic responses were measured using impact testing. The sample rate of the data acquisition is set to 200Hz; signals were recorded during 8 seconds after the introduction of impact. The measurements are set with a quite dense grid (Δ=14.55 cm, Figure 3) for the sake of studying damage localization later. There are 45 impact points at each side of the slabs and three accelerometers (Ref 1-Ref 3 in Figure 3) are used to capture dynamic responses. So, in each condition, we have 3 sets of data containing 90 signals.

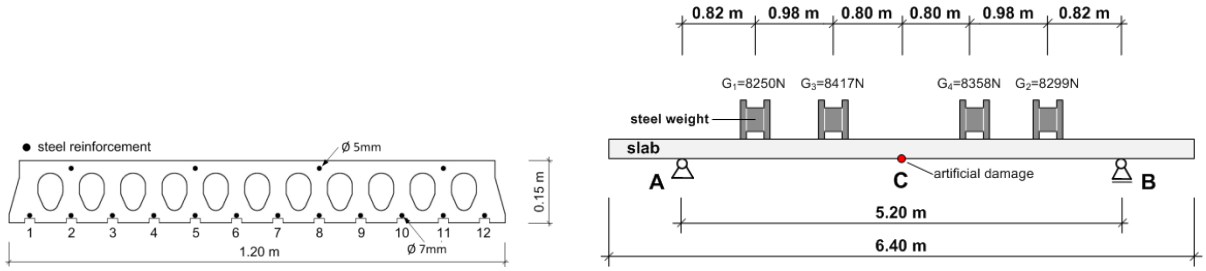

a) Cross-section of the panels in section C b) Scheme of loading and location of cracks (point C)

Figure 2 - Panel structure and experiment scheme

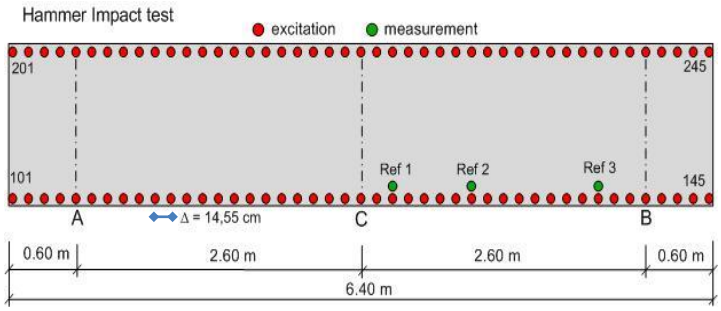

Figure 3 - Measurement setup: impact point (101-145 and 201-245) and accelerometer positions (Ref 1 - Ref 3)

Damages were introduced by static mass loading (Figure 2b), cutting of steel wires and are given in Table 1. Table 2 summarizes observations during the crack forming until the collapse in both types of slabs.

Table 1 - Damage scenarios

No	Damage scenario	Cutting percentage in cross-section C	Remark
#0	Intact state – no damage	-	Later we consider states #0, #0*, #1*, #2*, #3*. * denotes a state after loading and then removing of 4 heavy weights from the slab (shown in Figure 2b)
#1	Cutting of 2 tendons (n^0 6,7 - refer to Figure 2a)	16.7%	
#2	Cutting of 4 tendons (n^0 6, 7, 2, 11)	33.3%	
#3	Cutting of 6 tendons (n^0 6, 7, 2, 11, 4, 9)	50%	
#4	Cutting of 8 tendons (n^0 6, 7, 2, 11, 4, 9, 3, 10)	66.7%	

Table 2 - Description of damages

No.	Reinforced concrete (RC) slab	Prestressed concrete (PC) slab
#0	No damage	No damage
#0*	Appearance of a decisive crack pattern in the middle of the slab, large creep	No crack observed
#1*	No further cracks, current cracks grow and also creep	No crack observed, no considerable deformation
#2*	As above	Appearance of a hairline crack in the middle of the slab, minimal deformation
#3*	As above	As above
#4*	Collapse	Collapse

5.2 Modal identification results

Both the SSI and PolyMax methods were applied in this work to assess their performances. 10 block rows are used in the SSI analysis. At a first glance, a great difference is observed between the stabilization diagrams of the two methods as shown in Figure 4, when considering the healthy state of the reinforced concrete (RC) slab by set of measurement 1 (the data was collected at position Ref 1 in Figure 3).

The SSI diagram shows several stablized poles with small damping. Many poles with high damping are present and there exists some stabilized poles which are quite close to each other. For example, in the range [40Hz-50Hz], there are at least three modes at about 40Hz, 45.5Hz and 50Hz. The two first modes arround 11Hz and 40Hz show clearly bending shapes as illustrated in Figure 5; the modes at 45-46 Hz and at 50 Hz are very similar and correspond to a bending-torsion mode-shape. However, the mode-shape at 50 Hz looks rougher, which indicates that it is possibly a parasite of mode at 45Hz.

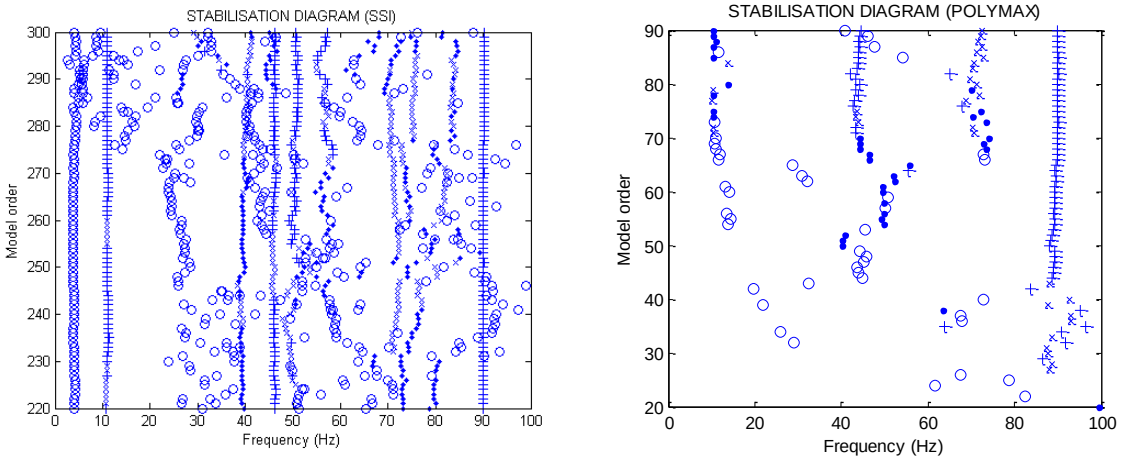

Figure 4 - Stabilization diagrams from the SSI and PolyMax methods

Using PolyMax, the stabilization diagram is very clear as spurious modes of negative damping ratio are excluded. Identified modes can be easily picked out as only a few stabilized poles are outlined. However, modes in the interested frequency band [0-50Hz] appear quite lately at high model orders. The shapes of the first two bending modes are presented in Figure 6 and are in good agreement with the SSI results. If we have a look at the third mode-shapes, we note that the displacements at the bearings are quite important. This may indicate that in actual conditions, the slab is not well fixed at the bearings.

Comparing the results in terms of shapes, the modes-shapes provided by the PolyMax method look smoother. This may rely on the type of data used as input by the methods. For SSI, raw time data including noise are used directly. For PolyMax, frequency-domain data are used as input, which allows selecting data in the frequency range of interest and thus eliminating noise and unconcerned modes.

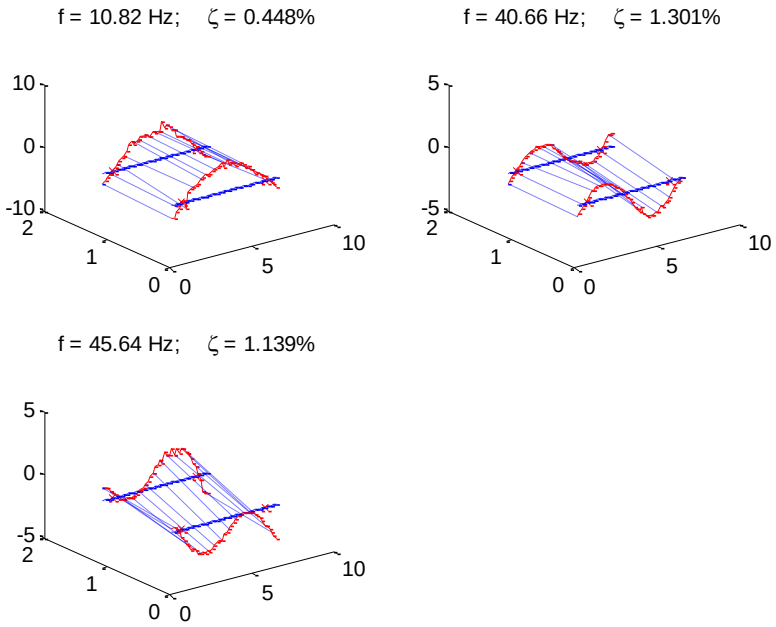

Figure 5 - Mode-shapes identified by SSI, points with x denoted bearing positions (axe A, B in Figure 3)

Another difference between the two methods relies in the possibility of well identifying specific modes. It can be noted that the PolyMax method gives damping ratios that are generally higher than in the SSI method. For example, mode 1 (around 11Hz) is steadily identified by SSI with a low damping value, while it is much more delicate to identify by the PolyMax method. As shown in Figure 4, if the PolyMax method is used in the entire frequency range, modes at 45Hz and 90Hz stabilize very early (as they are dominant due to their low damping value), which renders the identification of mode 1 less obvious and even impossible in the case of damage #1*.

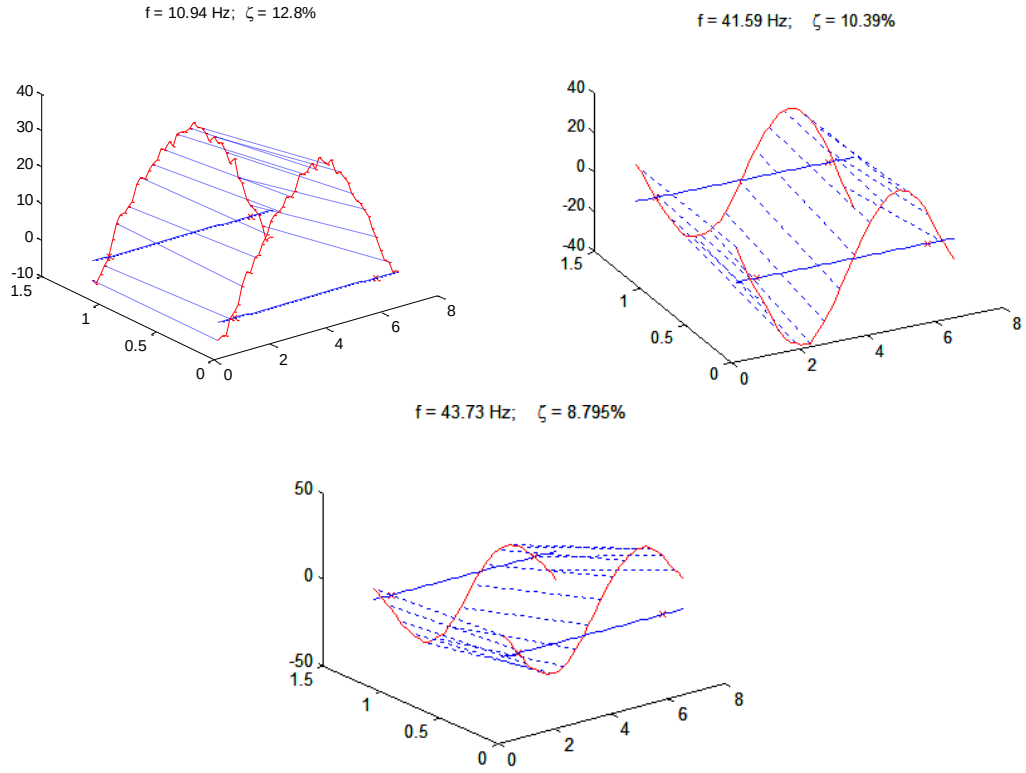

Figure 6 - Mode-shapes identified by PolyMax

Identification results of the first eigenfrequency using different methods are reported in Table 3 for both the reinforced (RC) and prestressed (PC) concrete slabs for all conditions.

Table 3 - The shift of the first frequency (Hz) from the intact state until before the collapse

	RC slab					PC slab				
State	#0	#0*	#1*	#2*	#3*	#0	#0*	#1*	#2*	#3*
f by peak picking	10.9	8.94	7.76	7.6	7.4	11.75	11.70	11.65	11.65	11.55
f by SSI	10.82	9.20	8.00	7.70	7.35	11.73	11.84	11.61	11.69	11.33
f by PolyMax	10.94	9.00	//	//	//	11.74	11.70	11.63	//	//

For illustration purposes, the stabilization diagrams are presented in Figure 7 for damage #3* in the RC slab. Using SSI, eigenfrequencies are identified at 7.35Hz, 35Hz, 44Hz and 46.7Hz in the range [0-50Hz]. The first two modes correspond to bending and the next two modes are torsion modes. Parasite poles exist, especially near 35Hz. In the other hand, based on the PolyMax, with increasing damages, more and more bending mode is declined, torsion becomes dominant mode in the range [40Hz-50Hz].

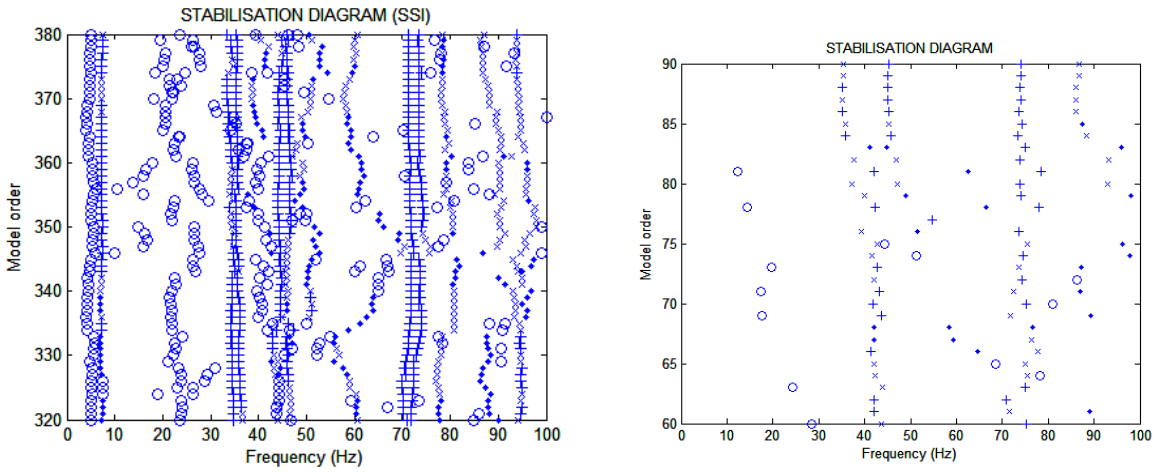

Figure 7 – Stabilization diagrams from SSI (left) and PolyMax (right) for damage #3*

Table 3 shows a clear decrease of the first resonance frequency of the RC slab as the level of damage increases. However, for the PC slab, the first eigenfrequency varies only slightly between the different conditions; only the healthy state (#0) and the state before the failure (#3*) are clearly distinct. This is consistent with the observations and cracking described in Table 2: no change is noticed between state #0 to #1*. In comparison with the RC slab, apparent damage occurs very lately in the PC slab; the crack initiation and hence the deformation remains negligible until failure, which makes the detection more difficult.

5.3 Damage detection based on the concept of subspace angle

The different conditions in the slabs may also be detected using the concept of subspace angle. In this section, the Enhanced Principal Component Analysis (EPCA) method is applied as it can provide dynamical subspaces (active principal components) without relying on modal identification results. For the RC slab, apart from damage cited above: #0*, #1*, #2*, #3*, the healthy state is also compared with conditions #0a, #0b (‘a’ and ‘b’ denote the states after loading of 2 and 3 steel weights respectively). According to theoretical calculation, the cracking load should be reached from the loading of 2 steel weights, without cutting any wire. The EPCA detection results are quite stable with different model orders and presented in Figure 8a. From state #0a when the cracking load is reached, the subspace angle is high. Damage indices increase visibly when the cutting of wires progresses.

As the first mode is not identified by Polymax for damage #1*, the detection is based only on the second mode. The results are presented in Figure 8b.

For the prestressed concrete slab (PC), the detection results are shown in Figure 9. As noted previously, the frequency variation is very small between the different damage conditions of the PC slab and only a little hairline crack was observed for damage #2*. In Figure 9, subspace angles obtained by the EPCA method increase proportionally following the damage levels. PolyMax shows the smallest index for damage #1* but the last level #3* is clearly distinct from the other conditions.

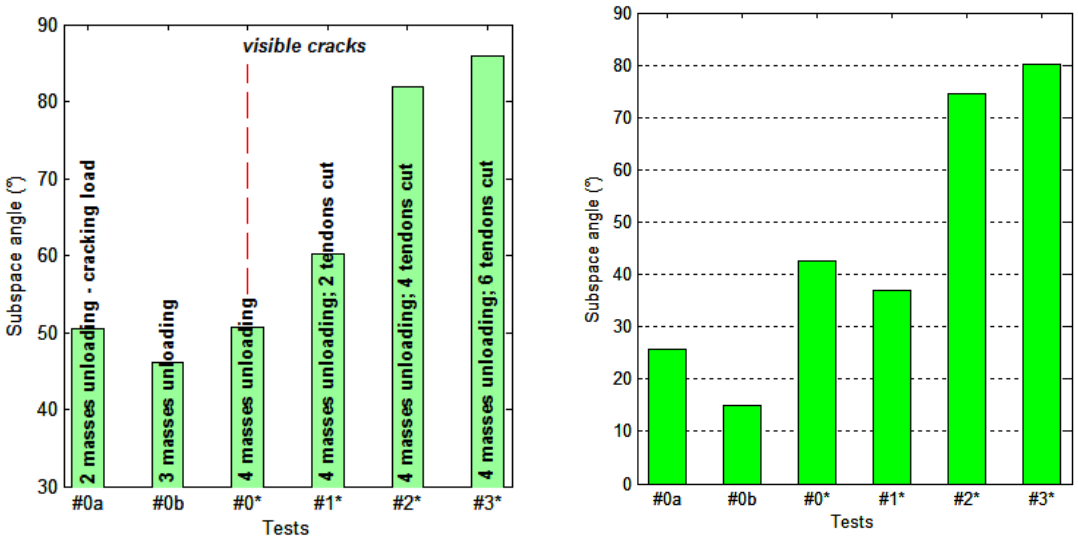

a) EPCA detection b) PolyMax detection

Figure 8 – Damage detection for the RC slab

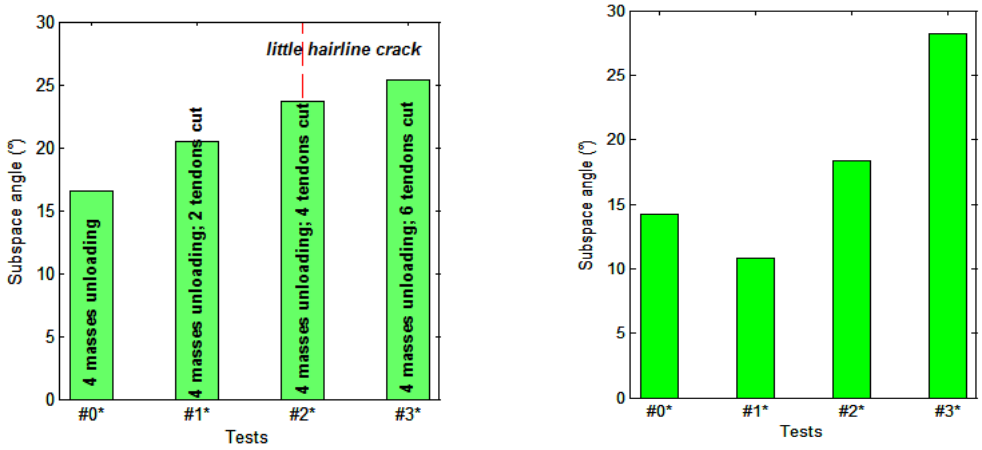

a) EPCA detection b) PolyMax detection

Figure 9 – Damage detection for the PC slab

5.4 Damage localization

As shown in Table 2, damage produces a crack pattern in the middle of the slab. So it is expected that the damage localization procedure will point out damage around this zone, i.e. along axis C passing through point 23 (see Figure 3) marking the middle of the slab. For the sake of conciseness, only the signals coming from one slab side are used here (from point 101 to 145 in Figure 3).

5.4.1 Localization method based on flexibility

For each condition of the structure, the flexibility matrix is determined using Equation (4). Further details are presented in [16]. In this section, the modal parameters are estimated using the global polynomial method available in the ME'scope Software.

The square of eigenfrequencies in the denominator of Equation (4) shows that the first eigenmodes are predominant for the flexibility matrix. In this example, the influence of the first mode is capital. As the amplitude of the corresponding mode-shape is the largest in the middle of the slabs, this zone is the most flexible. Figure 10 represents the diagonal elements of the flexibility matrices for both the RC and PC slabs. It is observed that the flexibility increases with increasing damages. The differences from the reference state #0* are given in Figure 11.

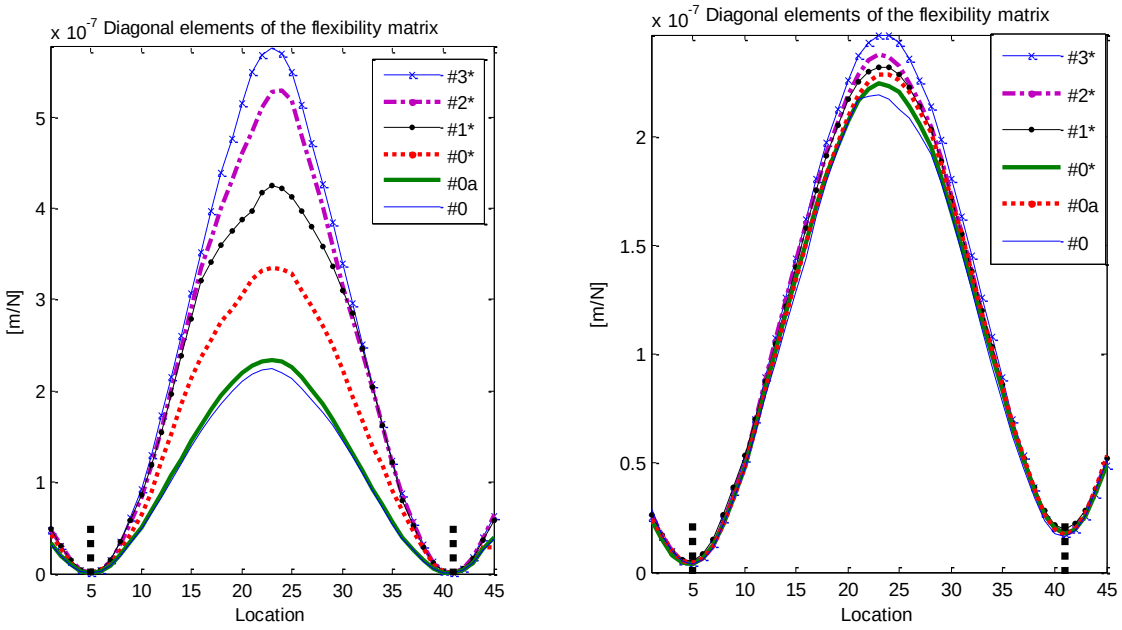

a) For the reinforced concrete (RC) slab b) For the prestressed concrete (PC) slab

Figure 10 – Diagonal entries of the flexibility matrices

The damage indicator δ_i in Equation (5) is also examined and presented in Figure 12. All the results above show the highest indices at the middle of the slab where damage is located. Moreover, damage levels are well distinguished. With respect to the RC slab, the detection in the PC slab is less explicit for weak damages. Figure 10b shows that the introduced damages do not induce considerable variations of the flexibility for the PC slab. The difference between the damage states remains small so that flexibilities for damage states #0a and #0* are not proportional to the levels of damage.

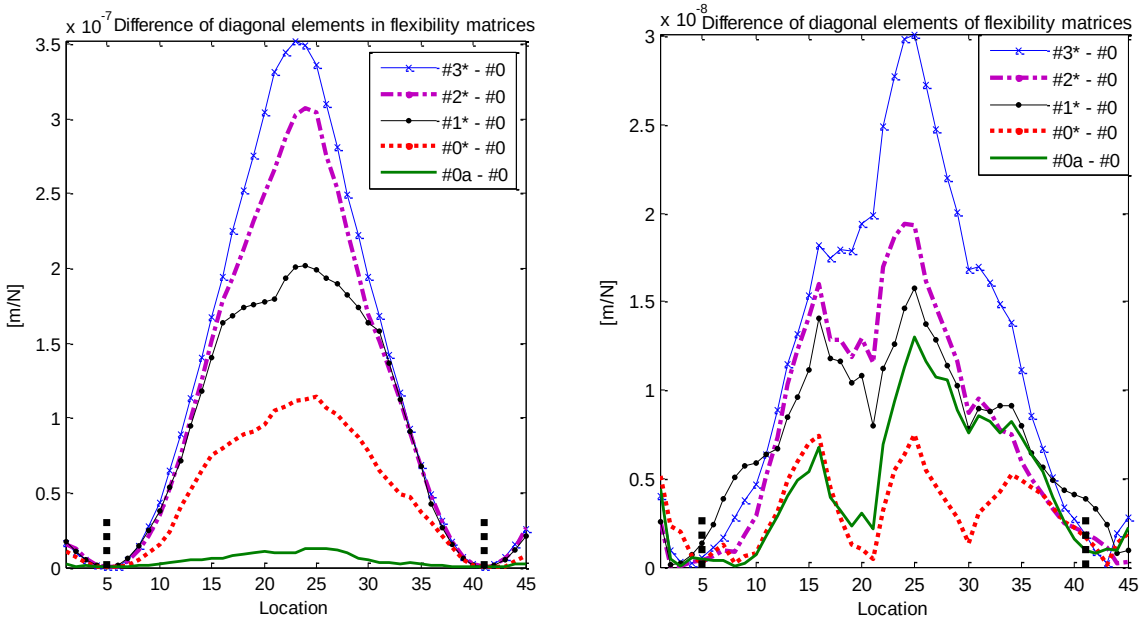

a) For the RC slab b) For the PC slab

Figure 11 – Difference of diagonal entries

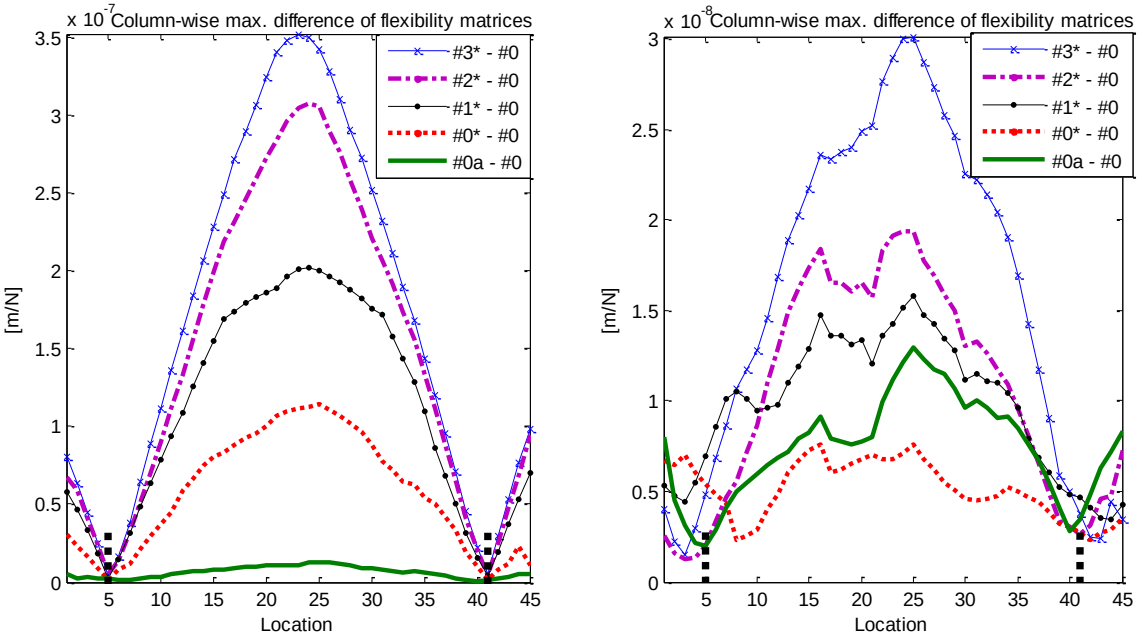

a) For the RC slab b) For the PC slab

Figure 12 – Maximum values of each column of flexibility difference

The relative difference according to Equation (6) is represented in Figure 13. Similar observations are obtained in Figure 14 for the relative difference performed from maximum

value of each matrix column. However, damage #3* in the PC slab is much better revealed in this figure than in Figure 13.

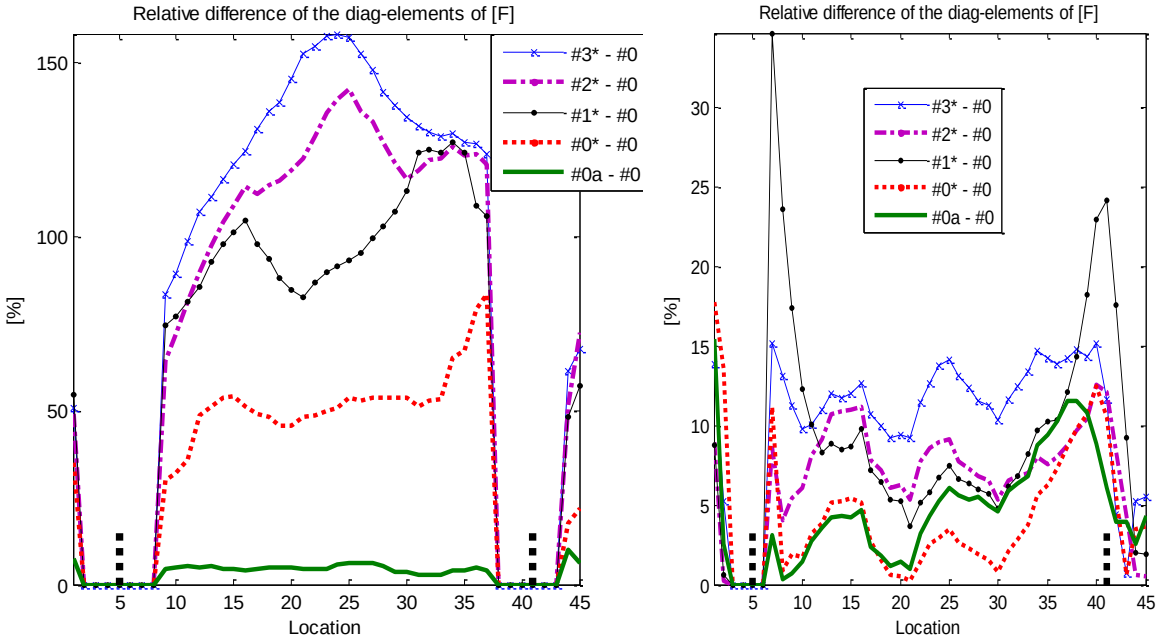

a) For the RC slab b) For the PC slab

Figure 13 – Relative difference between the diagonal entries of flexibility matrices

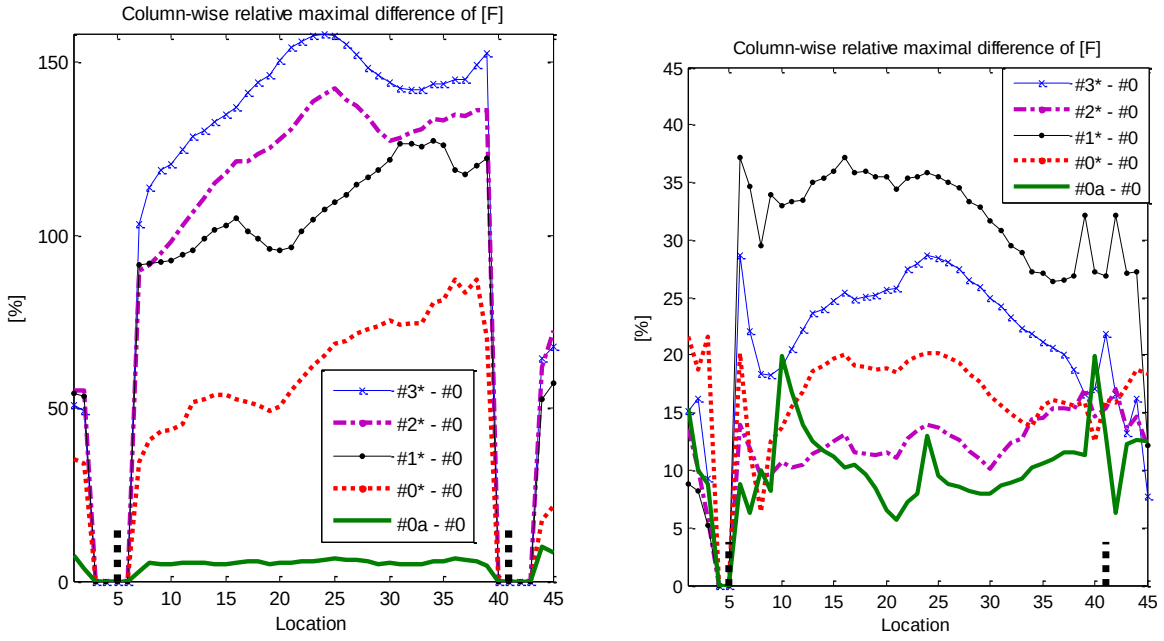

a) For the RC slab b) For the PC slab

Figure 14 – Relative difference between maximum values of each flexibility column

5.4.2 Method based on the sensitivity analysis of PCA results

Let us recall that in PCA, a large number of data is one of the requirements so that a principal component in matrix **U** (Equation 8) converges to a representative vector; for this reason, the frequency range should be chosen large enough to get sufficient observation data in $\mathbf{H}^s(\omega)$. For the RC slab, the frequency range [4 Hz – 26 Hz] corresponding to mode 1, is first selected to eliminate low-frequency noise and higher frequency modes. The results for $\left|\Delta\frac{\partial U_1}{\partial p_k}\right|$ shown in Figure 15 are obtained from the set of measurement n°3. As the sensor was located at point 38 for this set of measurement, parameter p_k is chosen to correspond to k_{38} - 38th element of the 'experimental' stiffness matrix. The 'undamaged' vector of $\partial U_1/\partial p_k$ is extracted from state #0 which is considered as reference. Based on the sensitivity of mode 1, damage in the RC slab can be located from state #2*, as the highest peaks of the indicator vector are found close to point 23 (axe C) where the cracks gather.

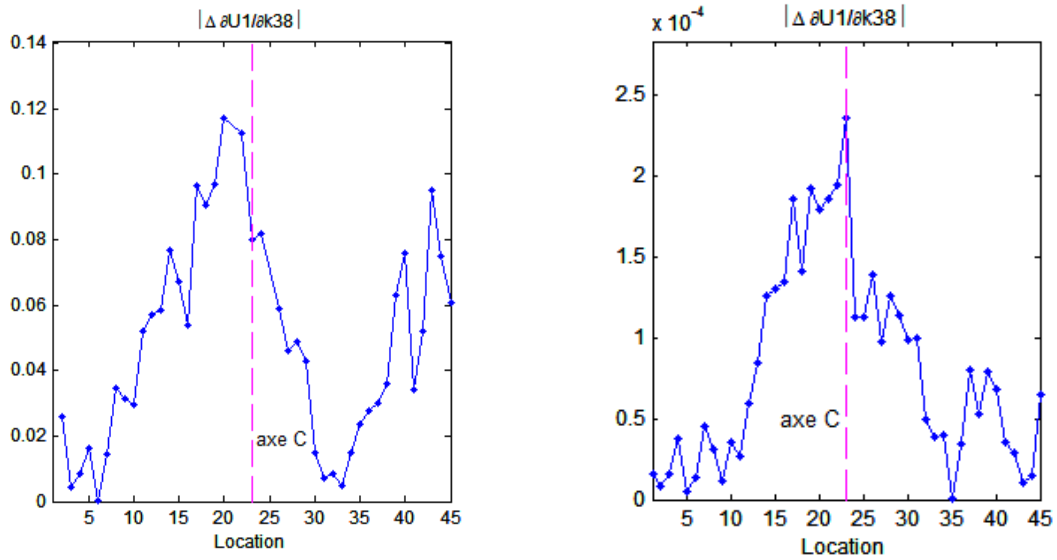

a) For damage #3* b) For damage #2*

Figure 15 – Damage localization in the RC slab, based on mode 1

To take into account higher frequency components (mode 2), the frequency range [4Hz – 50Hz] is now considered. Using this range, the second bending mode which also more sensitive to damage is dominant. All damages are accurately located as shown in Figure 16.

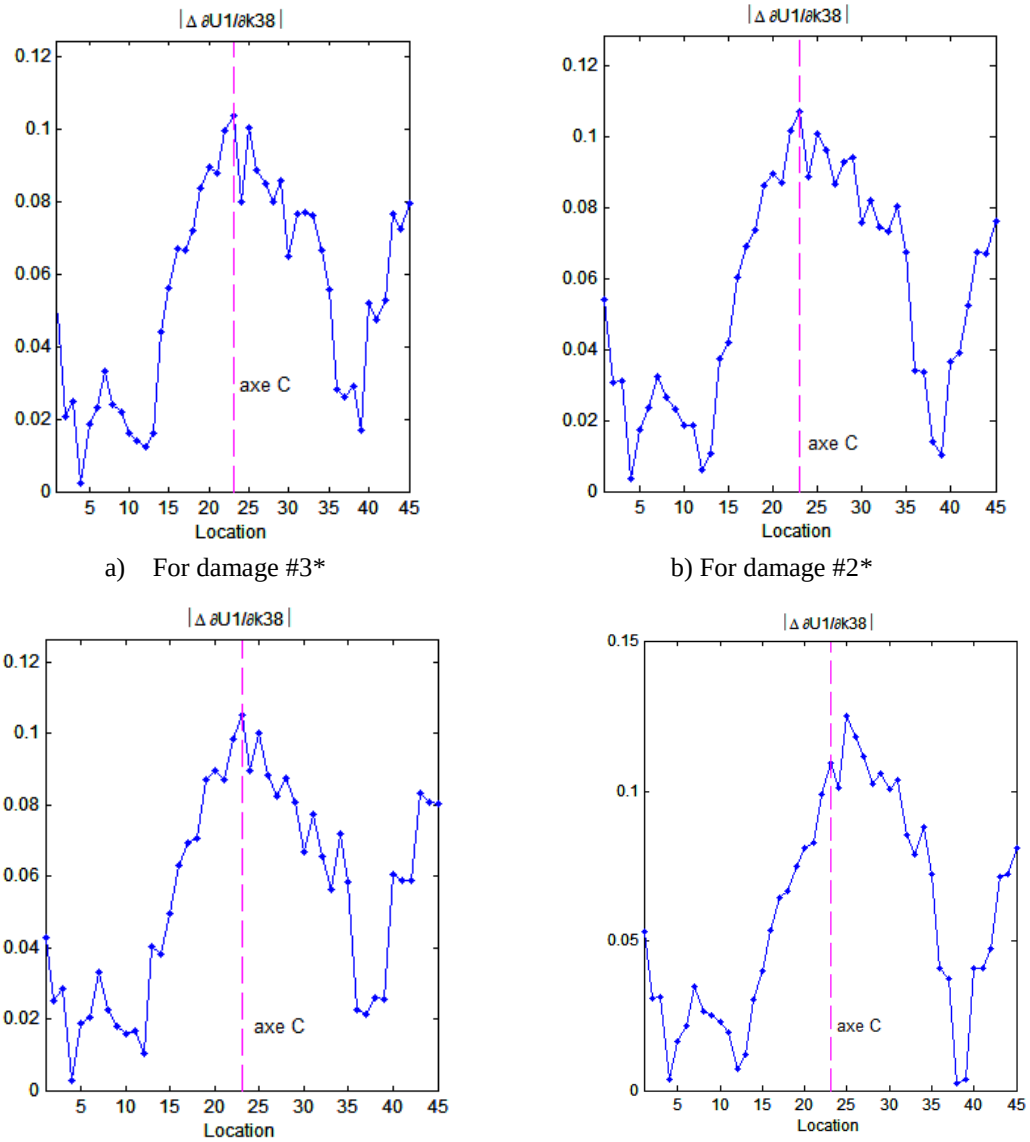

a) For damage #3* b) For damage #2*

c) For damage #1* d) For damage #0*

Figure 16 – Damage localization in the RC slab, based on mode 2

In the case of the PC slab, damages are detected much later and are less apparent than in the RC slab. The localization procedure does not give any interesting outcome for the PC slab when mode 1 is considered. However, as in the RC slab, the use of mode 2 allows a better localization. Damages #3* and #2* are better located than damage #1* as shown in Figure 17. The peaks do not arise exactly at point 23 (along axis C) but in the neighboring area.

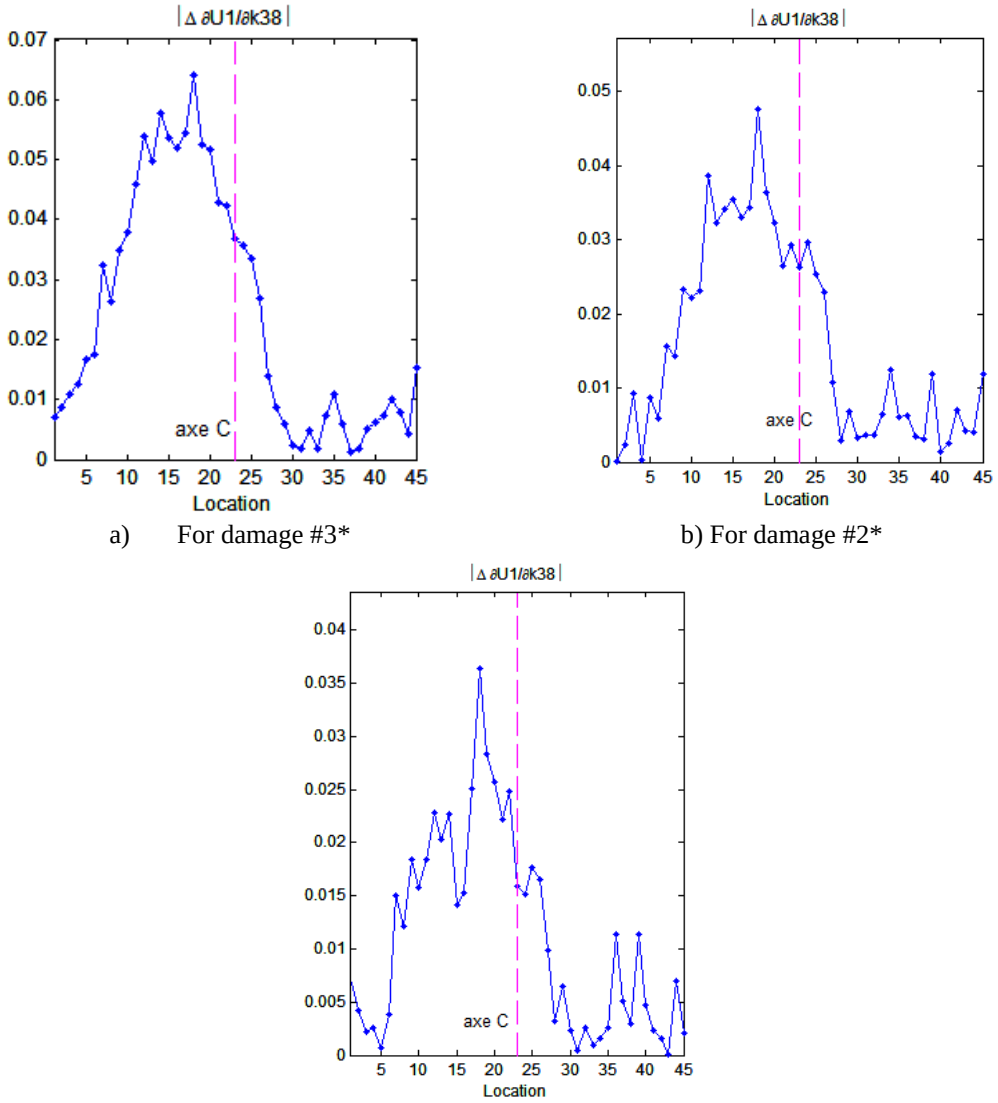

a) For damage #3* b) For damage #2*

c) For damage #1*

Figure 17 - Damage localization in the PC slab, based on mode 2

6 CONCLUSION

In this paper, both stochastic subspace algorithms in the time-domain and identification in the frequency-domain are dealt with to perform damage detection. The advantage of blind identification methods from output-only measurements relies in its simplicity and practical use. Besides, the PolyMax method results in much clearer stabilization diagrams. The application of both methods on the example of progressively damaged concrete slabs revealed the capability of the SSI method to perform good identification in a large variety of damage conditions. The damage detection method based on flexibility gives important information on

the level of damages. Finally, the damages are well located using the sensitivity analysis of PCA results even for low levels of damage in both the RC and PC slabs.

ACKNOWLEDGMENT

The author Viet Ha Nguyen is supported by the National Research Fund, Luxembourg which is gratefully acknowledged.

REFERENCES

[1] B. Peeters, G. De Roeck, *Stochastic System Identification for Operational Modal Analysis: A Review*, Journal of Dynamic Systems, Measurement and Control, Transaction of the ASME, vol 123, 2001, pp. 659-667.

[2] V.H. Nguyen, C. Rutten, J.-C. Golinval, *Fault Diagnosis in Industrial Systems Based on Blind Source Separation Techniques Using One Single Vibration Sensor*, Shock & Vibration 5, 2012, pp. 795-801.

[3] A.-M. Yan, J.-C. Golinval, *Null subspace-based damage detection of structures using vibration measurements*, Mechanical Systems and Signal Processing 20, 2006, pp. 611-626.

[4] V.H. Nguyen, *Damage Detection and Fault Diagnosis in Mechanical Systems using Vibra tion Signals*, 2010, PhD dissertation, University of Liège.

[5] B. Peeters, G. Lowet, H. Van der Auweraer, J. Leuridan, *A new procedure for modal parameter estimation*, Sound and Vibration/January 2004.

[6] B. Peeters, H. Van der Auweraer, *PolyMAX: A revolution in operational modal analysis*, Proceedings of the 1st international operational modal analysis conference 2005, Copenhagen, Denmark, April, pp. 41–52.

[7] B. Peeters, S. Pauwels, J. Debille, *Enhanced exploitation of vibration test data by the PolyMax modal parameter estimation method*, Proceedings of the 5th International Symposium on environmental testing for space programs, June 2004, Noordwijk, The Netherlands.

[8] B. Peeters, F. Vanhollebeke, H. Van der Auweraer, *Operational PolyMAX for estimating the dynamic properties of a stadium structure during a football game*, IMAC-XXIII: Conference & Exposition on Structural Dynamics, 2005, Orlando, Florida, USA.

[9] G.H. Golub, C.F. Van Loan, *Matrix computations*, Baltimore, The Johns Hopkins University Press, 1996.

[10] A. Yan, J.-C. Golinval, *Structural damage localization by combining flexibility and stiffness methods*, Engineering Structures 27(2005), pp. 1752-1761.

[11] J. Mahowald, S. Maas, D. Waldmann, A. Zuerbes, F. Scherbaum, *Damage identification and localisation using changes in modal parameters for civil engineering structures*, Proceedings ISMA 2012, Leuven, Belgium.

[12] A.K. Pandey, M. Biswas & M. M. Samman, *Damage detection from changes in curvature mode shapes*, Journal of Sound and vibration, 142, (1991), pp. 321-332.

[13] V.H. Nguyen, J.-C. Golinval, *Localization and quantification of damage in beam-like structures using sensitivities of principal component analysis results*, Mechanical Systems and Signal Processing 24(6), 2010, pp. 1831-1843.

[14] J.L. Junkins and Y. Kim, *Introduction to Dynamics and Control of Flexible Structures*, AIAA Education Series, Reston, VA, 1993.

[15] J. Mahowald, V. Bungard, D. Waldmann, S. Maas, A. Zürbes, G. De Roeck, *Comparison of linear and nonlinear static and dynamic behaviour of prestressed and non-prestressed concrete slab elements*, Proceedings of The International Conference on Noise and Vibration Engineering 2010, Leuven, Belgium, pp. 717–728.

[16] J. Mahowald, *Evaluation of dynamic damage indicators on real-life civil engineering structures: measurement uncertainty and environmental influences considered*, 2013, PhD Dissertation, University of Luxembourg.